Journal of Biomolecular NMR, 3 (1993) 495–513
ESCOM



J-Bio NMR 138

# High-resolution structure and dynamic implications for a double-helical gramicidin A conformer

S.M. Pascal and T.A. Cross*

*Institute of Molecular Biophysics and Department of Chemistry, Florida State University, Tallahassee, FL 32306-3006, U.S.A.*

Received 6 March 1993
Accepted 31 May 1993

*Keywords:* 2D NMR; NOE; Coupling constant; Distance geometry; Simulated annealing; Gramicidin; Peptide structure; Peptide dynamics

## SUMMARY

The high-resolution structure of a dimeric conformer of gramicidin A, a 15-residue polypeptide, has been determined in the mixed-solvent system of benzene and ethanol by 2D NMR techniques. NOEs, coupling constants and hydrogen-bond information were used to generate 744 experimental constraints for the dimer. Stereoassignment of most β-methylene groups was achieved by analysis of $^3J_{\alpha\beta}$, $d_{\alpha\beta}(i,i)$, $d_{N\beta}(i,i)$ and $d_{N\beta}(i+1,i)$ distances, and consideration of the initial backbone structure determinations. Stereoassignment of several leucine methyl groups was accomplished via a distance geometry/simulated annealing routine, used for structure determination and refinement. The relatively static backbone structure was determined first and held rigid while side-chain conformations were calculated. This procedure is evaluated versus standard NMR structure determination protocols. The backbone is an antiparallel intertwined double helix, with 5.6–5.7 residues per turn, a total dimer length of 36–37 Å, and a pore width of 2.5–3.0 Å (van der Waals to van der Waals). The structure and dynamics of the side chains are discussed in depth, with careful attention for both the convergence of structures and the residual constraint violations per residue. Side-chain positions impart substantial amphipathic character to the helix, which could influence the conformational change that takes place upon membrane insertion of this channel-forming polypeptide.

## INTRODUCTION

Through achieving a very highly constrained polypeptide structure it is possible to develop a model for large-amplitude dynamics (when present) and to improve the protocols for structural refinement. The linear peptide gramicidin A takes on a variety of conformations in organic solvents. In the mixed-solvent system of benzene and ethanol, a single conformer is dominant and the polypeptide backbone has been characterized (Zhang et al., 1992). Using distance and torsion-angle constraints it has been possible to determine side-chain conformations with very small

*To whom correspondence should be addressed.

rmsd differences between structures. The residual NOE violations can then be used to obtain a qualitative estimate of the local dynamics in the side chains. This separation of structural and dynamic information is one of the greatest challenges in NMR (Torda et al., 1990; Brüschweiler et al., 1991). The approach presented here utilizes the rigidity of the helical backbone relative to the more mobile side chains. NOEs involving only the backbone are then virtually free from dynamic effects, and can thus be introduced earlier in the refinement procedure. NOEs involving side-chain protons are introduced only after the backbone conformation has been determined. Violation of NOEs between side-chain protons and the backbone can then be used to gauge dynamics, via the conformational range necessary to eliminate these violations. This approach does not require a detailed heteronuclear relaxation study and in fact provides largely complementary information. Knowledge of the dynamics can then be used to evaluate the quality of the structure and obtain an indication of the influence of dynamics upon NMR structure determination in general.

Short linear peptides are generally disordered in aqueous solution. Too few amino acid residues are present to allow formation of a stable hydrophobic core and hydrophilic surface. However, the C-peptide of ribonuclease A (13 residues) has been shown to form an α-helix in water at low temperatures (Brown and Klee, 1971). Other peptides which form helices and β-turns in aqueous solution have also been found (Dyson et al., 1985, 1988; Williamson et al., 1986), although most of these peptides contain either disulfide linkages or proline residues, which reduce the conformational freedom. Addition of TFE to aqueous solutions reduces the dielectric constant and helps induce α-helical structure in certain peptides (Lynch and Kaiser, 1988; Breeze et al., 1991). It is, however, unusual to find a significant degree of secondary structure in a short linear peptide without these added factors, let alone a single very stable structure such as that for gramicidin in benzene/ethanol.

Gramicidin A is a 15-amino acid residue polypeptide (CHO-L-Val-Gly-L-Ala-D-Leu-L-Ala-D-Val-L-Val-D-Val-L-Trp-D-Leu-L-Trp-D-Leu-L-Trp-D-Leu-L-Trp-$NHCH_2CH_2OH$) produced enzymatically during sporulation by *Bacillus brevis*. The alternating LD-stereochemistry allows gramicidin to form β-helices; i.e. essentially a β-sheet structure with all side chains on one side of the sheet, thereby inducing the formation of a helix (Ramachandran and Chandrasekaran, 1972). The apolar nature of the side chains creates a hydrophobic solvent-accessible surface, and the helical backbone forms a small hydrophilic core.

Gramicidin is one of the few polypeptides with a dual physiological role. The lytic role of gramicidin as a monovalent cation-selective channel has been studied extensively (Katz and Demain, 1977; Anderson, 1984; Killian, 1992). A wide variety of spectroscopic data, scattering data and molecular modeling has shown that the lytic form of gramicidin in the lipid bilayer is a formyl-end-to-formyl-end membrane-spanning β-helical dimer. The helical sense is right-handed (Nicholson and Cross, 1989) and the helical pitch is that of a single-stranded helix (Katsaras et al., 1992). Through extensive molecular-modeling efforts, the folding motif for the channel conformation is well accepted, but a complete experimental structure determination has yet to be achieved. A regulatory role for gramicidin in switching *Bacillus brevis* from vegetative growth to sporulation, which involves binding to the σ subunit of the RNA polymerase, has also been established (Sarkar et al., 1977; Fisher and Blumenthal, 1982). However, little is known about this conformation of gramicidin.

The behavior of gramicidin in organic-solvent environments has also been extensively studied.

Two-dimensional (2D) NMR studies of gramicidin in dimethyl sulfoxide gave no evidence of a stable conformation (Roux et al., 1990; Pascal and Cross, unpublished results; Taylor and Koeppe, personal communication). Ethanol, however, induces a heterogeneous mixture of several well-ordered dimers (Veatch et al., 1974). Infrared spectroscopy, circular dichroism and 1D NMR studies suggested that these dimers consist of four different intertwined β-helices. Backbone folding motifs for these four dimers, designated species 1, 2, 3 and 4, have been determined by analysis of 2D NMR spectra of the conformational mixture in ethanol (Bystrov and Arseniev, 1988). Recently, a more detailed analysis for species 4, a right-handed parallel double-helical structure, has been achieved (Pascal and Cross, 1992). The species 3 conformer, a left-handed antiparallel double helix, has been observed in several environments. X-ray diffraction studies of crystals out of benzene/ethanol (Langs, 1988) and methanol (Langs et al., 1991) yielded two high-resolution structures for this species, with small but significant differences. Crystallization out of methanol and redissolution in dioxane also produces a species 3 folding motif, as determined by NMR techniques (Arseniev et al., 1984).

In this study, addition of benzene to ethanol is used to produce an environment which causes species 3 to dominate the conformational equilibrium (> 90%, Zhang et al., 1992). This species is used as a model to investigate surface dynamics and structure-determination methods as described above. The conformation in benzene/ethanol is also interesting from other points of view. The preceding paragraph demonstrates that interactions between the solvent molecules and the polypeptide play a crucial role in the folding process. The combined information of gramicidin conformation and dynamics in different environments may provide clues which can help to clarify this role. Also, the left-handed double-helical species 3 structure converts readily to the right-handed single-stranded channel conformation upon hydration of dry preparations of gramicidin and lipid. Because of the well-documented solvent history dependence of such preparations (LoGrasso et al., 1988; Killian et al., 1988b) it is known that gramicidin does not adopt an unstructured monomeric state prior to the formation of the channel state. Speculation as to a membrane-insertion pathway has been described (Zhang et al., 1992). Information on the structure and dynamics of the benzene/ethanol conformation may lead to a clearer understanding of membrane insertion and the driving force for the conformational rearrangement.

Studies of peptides in organic solvents are proving to be fundamentally useful for understanding features of the membrane-lipid environment. Solvents such as dioxane and tetrahydrofuran can trap discrete gramicidin conformers (Braco et al., 1986; Pascal and Cross, 1992). Other solvents, such as ethanol and methanol, can promote the rapid interconversion of peptide conformers (Veatch et al., 1974). Even the addition of a few percent water to a trapping solvent can promote interconversion (Bano et al., 1989). Recently it has been shown that multiple conformations of gramicidin can be trapped in a lipid bilayer (Killian et al., 1988a; Cross et al., unpublished results). However, the multiplicity of gramicidin conformations observed in ethanol or methanol does not appear to be reproduced in the membrane environment (Pascal and Cross, 1993). Consequently, it appears that the bilayer environment has some of the properties of both of these extremes that have been described in organic solvents. Before detailed peptide–solvent interactions can be described both a structural and dynamic description of gramicidin in the solvent of interest is required. Here the detailed structure and the start of a dynamic description is presented.

## MATERIALS AND METHODS

*Sample preparation*

Gramicidin A was prepared by solid-phase peptide synthesis as described elsewhere (Fields et al., 1989). Synthetic gramicidin when cleaved from the solid-phase support was more than 98% pure as judged by HPLC and was used without further purification. The sample used for most NMR measurements consisted of 80 mg gramicidin A in 0.80 ml benzene-$d_6$ and 0.20 ml ethanol-$d_6$. Under these conditions, all nitrogen-bound hydrogens rapidly exchange with the ethanol OD, reaching a stable equilibrium at a ratio of approximately three deuterons to one proton. NOESY cross peaks not involving exchangeable resonances were measured from samples containing ethanol-$d_6$. The intensities of NOESY cross peaks involving exchangeable protons were reduced by a factor of approximately four in ethanol-$d_6$ (a factor of 16 in the case of HN–HN cross peaks) and so were more accurately determined by use of a second sample: 80 mg gramicidin A in 0.80 ml benzene-$d_6$ and 0.20 ml ethanol-$d_6$ ($CD_3CD_2OH$). Solvent suppression was not required.

*NMR spectra*

NMR spectra were recorded at a sample temperature of 30 °C on a 500 MHz Varian VXR500 spectrometer. Data were collected in phase-sensitive mode using the hypercomplex method (States et al., 1982). Typically, 8 192 $t_2$ points (4 096 real) and 512 $t_1$ increments (1 024 spectra) were collected. Spectra were zero-filled to 16 384 × 2 048 points. Recycle times were routinely set to 2.0 s. The HOHAHA (Braunschweiler and Ernst, 1983) experiment used a 110-ms MLEV-17 mixing scheme (Bax and Davis, 1985) with the transmitter power set to give a 90° proton pulse of 17.7 μs, and was acquired with 768 $t_1$ increments. The NOESY (Jeener et al., 1979; Kumar et al., 1980), canceled-diagonal NOESY (cdNOESY; Bodenhausen and Ernst, 1982) and randomized mixing time NOESY (rNOESY; Rance et al., 1985) experiments used for NOE measurements were obtained with 200-ms mixing times. Three-bond coupling constants were measured from DQF-COSY (Piantini et al., 1982; Shaka and Freeman, 1983) and P.E.COSY (Mueller, 1987) spectra. The residual benzene peak was used as a reference at 7.17 ppm.

## RESULTS

*Chemical-shift assignment*

The HOHAHA, DQF-COSY, P.E.COSY and NOESY spectra were used to confirm and complete the assignments published previously (Zhang et al., 1992). The backbone NOE pattern together with the existence of only one set of resonances, requires this conformation to be a fully symmetric dimer. Figure 1 shows the tryptophan $H_\alpha H_\beta$ region of the rNOESY and P.E.COSY spectra used to perform stereospecific assignments. Stereospecificity of all tryptophan and three of the four leucine β-methylene groups was determined after the final backbone structure determination, by analysis of $^3J_{\alpha\beta}$, $d_{\alpha\beta}(i,i)$, $d_{N\beta}(i,i)$ and $d_{N\beta}(i+1,i)$, in combination with van der Waals restrictions. Glycine $H_\alpha$ protons were assigned stereospecifically in an analogous manner, using $^3J_{N\alpha}$ and distances between the α-protons and other backbone protons. Stereospecific assignment of several leucine methyl groups was accomplished through the final structure calculations. The β-protons of $Leu^{12}$ have identical chemical shifts, obviating a stereospecific assignment. The $Val^1$

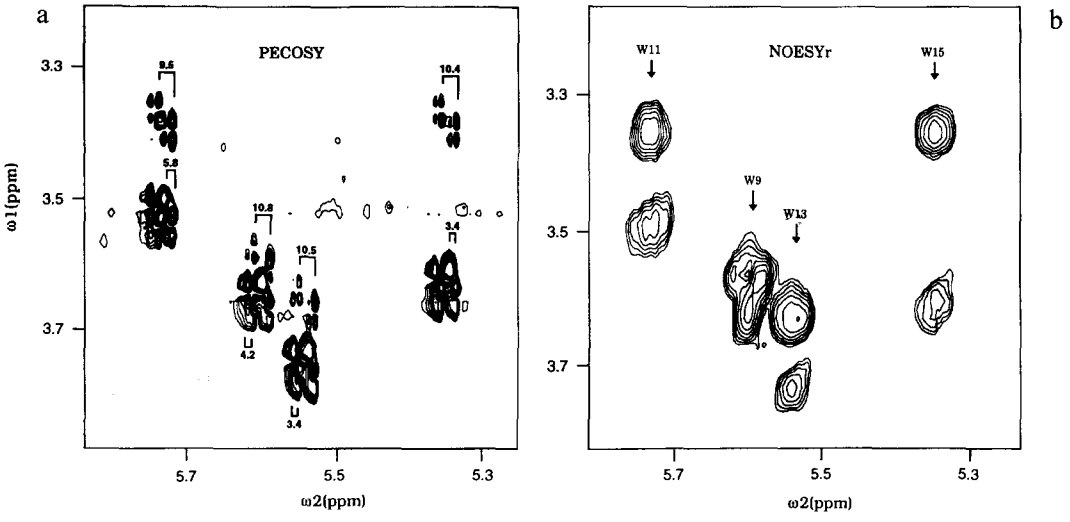


Fig. 1. Tryptophan $H_\alpha$–$H_\beta$ region of (a) P.E.COSY and (b) 200-ms mixing time rNOESY spectra of gramicidin A in benzene/ethanol. Values of passive coupling constants are shown. Stereospecificity of all tryptophan and three of the four leucine β-methylene groups was determined by analysis of $^3J_{\alpha\beta}$, $d_{\alpha\beta}(i,i)$, $d_{N\beta}(i,i)$ and $d_{N\beta}(i+1,i)$, together with van der Waals restrictions.

methyl groups are also degenerate. Assignment of the ethanolamine group remains incomplete due to chemical-shift degeneracy and rapid exchange of the OH proton with the solvent alcohol.

*Constraint determination*

Intensities of NOESY cross peaks were determined by volume integration using Varian VNMR sys4 software (version 2.2). Linear build-up rates were demonstrated by analysis of a series of NOESY experiments with mixing times of 100, 150, 200 and 250 ms for all cross peaks used as NOEs. Backbone distances were calibrated versus the glycine $H_\alpha$-$H_\alpha$ distance, and distances involving side chains were calibrated versus the tryptophan $H_{\varepsilon 1}$-$H_\delta$ cross peaks. NOEs corresponding to 630 distance constraints for the dimer were unambiguously assigned through use of the 200-ms NOESY, rNOESY and cdNOESY spectra. The rNOESY experiment (Fig. 1) was used to obtain accurate distances between protons separated by three bonds. This experiment employed a random variation of up to 10% of the mixing time, in order to eliminate unwanted COSY-type contributions in the cross peaks. The cdNOESY spectrum (Fig. 2) was extremely useful not only for the measurement of NOEs near the diagonal, but also in the crowded and intense methyl regions, where the $t_1$-noise and ridges were substantially reduced as compared to the standard NOESY spectrum.

NOEs were divided into four categories: 2.0–2.3, 2.0–2.7, 2.5–3.5 and 3.0–5.0 Å. Lower bounds for NOEs involving γ-, δ-, ε-, ζ- and η-protons were then set to 1.8 Å, to allow for effects of possible dynamics in the side chains (see Discussion). Hydrogen bonding information and helix sense have been determined previously (Zhang et al., 1992). Each hydrogen bond was converted into two distance constraints: $d_{HO}$ = 1.8–2.1 Å, $d_{NO}$ = 2.8–3.0 Å (Baker and Hubbard, 1984; Mitchell and Price, 1990). $^3J_{N\alpha}$ coupling constants were determined from the DQF-COSY spectrum by the method of Kim and Prestegard (1989), and $^3J_{\alpha\beta}$ couplings were measured as passive

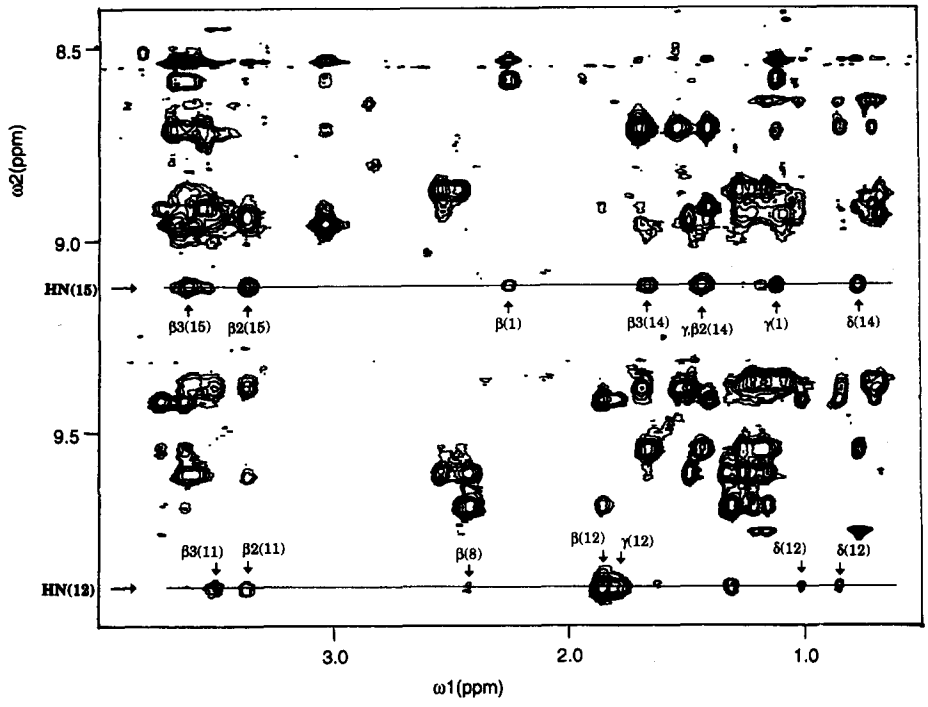


Fig. 2. HN-aliphatic region of cdNOESY spectrum with 200-ms mixing time. Cross peaks between two of the amide protons ($Trp^{15}$ and $Leu^{12}$) and the side chains are labeled.

couplings in P.E.COSY αβ cross peaks whenever possible (Fig. 1). Twenty-nine coupling constants were determined (Table 1) and converted into 44 dihedral constraints for the dimer. All valine $^3J_{\alpha\beta}$ couplings were intermediate in magnitude, and were thus not converted into constraints. Intermediate $^3J_{\alpha\beta}$ values might result from rapid dynamics about the $C_\alpha$–$C_\beta$ bond which would average large and small couplings (see Discussion). Uncertainty in measurement and interpretation of coupling constants was accounted for by an allowed 30° deviation of torsion angles from the calculated value.

To account for multiplicity, 1.0 Å was added to the upper limits for distances involving methyl groups or the degenerate $Leu^{12}$ β-protons. In both $Leu^4$ and $Leu^{14}$, one $H_\beta$ was nearly degenerate with the $H_\gamma$. NOEs to these protons could not be resolved, so they were treated as pseudoatoms (Wüthrich et al., 1983), with 1.5 Å added to the upper limits of distance constraints. Because of their chemical-shift degeneracy, the two methyl groups of $Val^1$ were treated as one pseudoatom encompassing six protons, with a total of 2.30 Å added to the upper-limit distances. The remaining methyl groups, which had not been stereospecifically assigned by specific coupling-constant and NOE observations ($Val^6$, $Val^7$, $Val^8$ and all leucines) were chemical-shift resolved from their stereopartners. Stereospecific assignment of these groups was arbitrarily done (downfield protons bound to carbons designated $C_{\gamma 3}$ or $C_{\delta 3}$), but chirality was randomly set at the start of the calculations and not restrained thereafter. This allowed the groups to invert if necessary, in order to satisfy the NOE constraints (Summers et al., 1990). This method eventually enabled the stereospecific assignments of $Leu^4$ and $Leu^{14}$ methyl groups (Table 1).

*Structure calculations*

Initial backbone structures were generated by distance geometry/simulated annealing using DSPACE (version 4.0). The routine was formally identical to a previously published procedure (Pascal and Cross, 1992), but in addition to $N_\alpha$ NOEs and hydrogen-bonding information, NN and αα NOEs were used here. NOE-derived $N_\alpha$ distances from a previous study (Zhang et al., 1992) were modified only slightly, due mostly to redefinition of distance categories. From 400 runs, 34 structures with a penalty function less than 6.0 were formed. Further refinement of these structures was performed via restrained molecular dynamics (Fig. 3) using X-PLOR (version 3.0). The backbone structure was determined and subsequently held rigid while the side-chain structures were calculated. This annealing protocol represents a modification of previously published routines (Nilges et al., 1988; Eberle et al., 1991). For the backbone, all experimental constraints ($N_\alpha$, NN and αα NOEs, hydrogen-bond distances, dihedral constraints from $^3J_{N\alpha}$ were treated as square-well potentials. Pseudo-force constants for coupling-constant, NOE and hydrogen bond-derived constraints were initially set to 10 kcal/mol.rad$^2$, 10 kcal/mol.Å$^2$ and 50 kcal/mol.Å$^2$, respectively. After 50 cycles of restrained conjugate-gradient minimization, van der Waals and electrostatic forces were replaced by a simple repulsive function during 3 ps of annealing at 600 K. Symmetry was then enforced between mirror backbone atoms of the dimer, and experimental

TABLE 1

$^1$H NMR CHEMICAL-SHIFT ASSIGNMENTS AND COUPLING CONSTANTS FOR GRAMICIDIN A SPECIES 3 IN BENZENE/ETHANOL

| Residue | $J_{NH\alpha H}$ | $J_{\alpha H\beta H2}$ | $J_{\alpha H\beta H3}$ | HN | $H_\alpha$ | $H_\beta$ | $H_\gamma$ | $H_\delta$ | $H_{\varepsilon 1}$ | $H_{\varepsilon 3}$ | $H_{\zeta 2}$ | $H_{\zeta 3}$ | $H_{\eta 2}$ |
|---|---|---|---|---|---|---|---|---|---|---|---|---|---|
| Val[1] | 9.4 | 7.3 | | 8.57 | 4.69 | 2.26 | 1.12[b] | | | | | | |
| Gly[2] | 3.6,8.0[a] | | | 8.63 | 3.56,5.08[a] | | | | | | | | |
| Ala[3] | 7.5 | | | 8.91 | 4.77 | 1.41 | | | | | | | |
| Leu[4] | 9.0 | 5.0 | 9.7 | 8.67 | 5.04 | 1.54,1.68[a] | 1.70 | 0.70,0.84[a] | | | | | |
| Ala[5] | 6.6 | | | 9.38 | 5.28 | 1.50 | | | | | | | |
| Val[6] | 10.0 | 5.6 | | 9.60 | 5.47 | 2.55 | 1.42,1.28 | | | | | | |
| Val[7] | 8.1 | 7.0 | | 8.87 | 5.25 | 2.48 | 1.23,1.17 | | | | | | |
| Val[8] | 9.4 | 7.0 | | 9.69 | 5.13 | 2.43 | 1.44,1.35 | | | | | | |
| Trp[9] | 8.6 | 4.2 | 10.8 | 9.61 | 5.62 | 3.60,3.64[a] | | 7.01 | 8.72 | 8.06 | 7.21 | 7.10 | 7.07 |
| Leu[10] | 9.0 | 3.4 | 10.4 | 9.37 | 5.09 | 1.12,1.24[a] | 1.18 | 0.74,0.67 | | | | | |
| Trp[11] | 8.4 | 5.8 | 9.5 | 8.94 | 5.76 | 3.39,3.52[a] | | 6.89 | 8.50 | 7.74 | 7.15 | 7.05 | 7.08 |
| Leu[12] | 9.3 | | | 9.89 | 5.00 | 1.87[b] | 1.80 | 1.02,0.86 | | | | | |
| Trp[13] | 6.4 | 3.4 | 10.5 | 9.40 | 5.57 | 3.65,3.74[a] | | 7.37 | 9.57 | 8.18 | 7.42 | 7.25 | 7.23 |
| Leu[14] | 9.8 | 4.1 | 11.2 | 9.53 | 5.12 | 1.44,1.67[a] | 1.43 | 1.19,0.77[a] | | | | | |
| Trp[15] | 7.3 | 3.4 | 10.4 | 9.09 | 5.36 | 3.37,3.62[a] | | 7.23 | 9.42 | 8.20 | 7.33 | 7.21 | 7.12 |
| Et[16] | | | | 8.93 | 3.65,3.01 | 3.53[c] | | | | | | | |
| Formyl | | | | 8.53 | | | | | | | | | |

Chemical shifts are expressed at 30 °C relative to benzene at 7.17 ppm.

[a] Sites where stereoassignments were made. Protons are listed in numerical order, i.e. $H_{\beta 2}$, $H_{\beta 3}$, using nomenclature from Demarco et al. (1978).

[b] Shifts of both groups are identifical.

[c] Shift of second β-proton is degenerate with either the first β- or an α-proton from ethanolamine. The OH proton exchanges rapidly with EtOD.

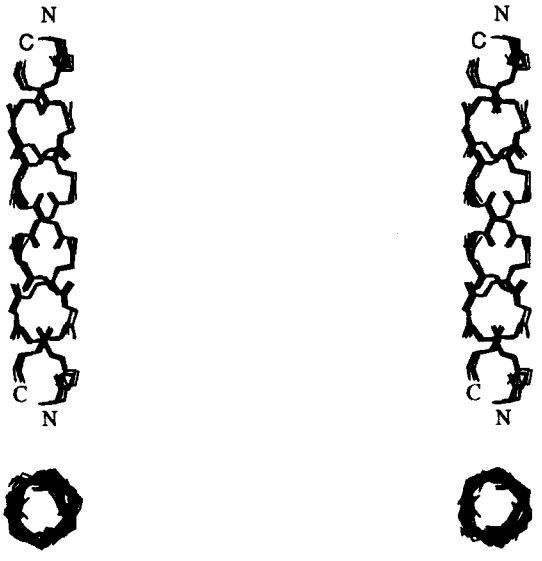


Fig. 3. Superposition of six backbone structures calculated by distance geometry/simulated annealing (stereoview). The helix is approximately 36 Å long with a pore diameter of approximately 2.7 Å.

force constants were linearly increased by a factor of three and the temperature linearly decreased to 300 K over a 5-ps annealing interval. Next, the van der Waals and electrostatic forces were reinvoked, and the experimental force constants were increased by a factor of two over a 12-ps interval at 300 K, followed by up to 1000 cycles of restrained minimization. The six lowest-energy backbone structures were retrained (Fig. 3).

The positions of the backbone atoms were then fixed, and the side chains were subjected to an analogous procedure, using $^3J_{\alpha\beta}$ coupling-constant information and all NOEs which involve side-chain atoms. Difficulty in simultaneously satisfying all side-chain NOE distances created violations of bond-angle and bond-length requirements in the side chains. These violations were removed through use of a refinement procedure (Nilges et al., 1992), applied only to the side-chain atoms, with the backbone fixed and symmetry enforced as above. This procedure combines slow cooling with a softening of the van der Waals repulsions, allowing close approach of nuclei to enable escape from local minima. The 15 lowest-energy structures used for analysis are shown in Fig. 4.

## DISCUSSION

*Average structure*

The backbone structure of gramicidin A in benzene/ethanol is a left-handed antiparallel double helix (Fig. 3). The helix continues to the ends of the dimer with only slight fraying. The periodicity is between 5.6 and 5.7 residues per turn. Dimers have a total length of 36–37 Å (formyl-O-to-formyl-O) and an average pore width between 2.5 and 3.0 Å (backbone van der Waals to van der Waals distance). Average backbone torsion angles are shown in Table 2. The rmsd values of $\phi$ and $\psi$ torsion anlges average about 10°. The rmsd of heavy backbone atoms in these six structures is

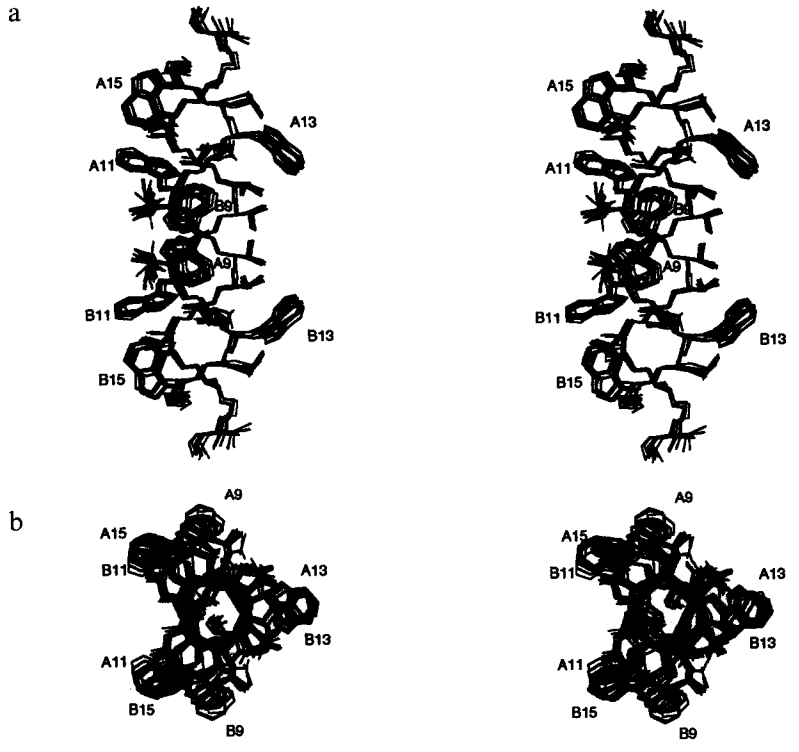


Fig. 4. Superposition of 15 side-chain structures built upon the six backbone structures of Fig. 3, calculated by distance geometry/simulated annealing: (a) side view (b) axial view. Tryptophan side chains from monomers A and B are labeled for reference. Four well-ordered valines (A7, A8, B7, B8) are shown in profile between A13 and B13. The disordered $Leu^{10}$ side chains are shown in profile between A11 and B11. Note also the side-chain-free groove on the left edge of the axial view. Protons and carbonyl oxygens are omitted for clarity (stereoview).

0.27 Å. Most carbonyl and amide groups in the backbone are involved in hydrogen bonds with other parts of the backbone (always between monomers). A hydrogen bond may form between $Leu^4$ HN and ethanolamine O, though its presence is difficult to detect due to incomplete chemical-shift assignment of $Et^{16}$. The $Gly^2$ HN and CO, as well as the formyl O and the indole nitrogen groups, are free to form hydrogen bonds with the solvent ethanol molecules.

Shown in Fig. 4 is the superposition of 15 complete structures gleaned from a series of structural calculations based on each of the six backbone structures with fixed geometry. The side-chain heavy-atom rmsd is 0.73 Å and the heavy-atom rmsd for the entire structure is 0.57 Å (see Table 2 for details). Most of the side chains have converged to a single rotameric state. $Trp^9$, $Trp^{13}$ and $Trp^{15}$ reside near the $\chi^1 = 180°$, $\chi^2 = -90°$ rotamer (Table 3). $Trp^{11}$ is near the $\chi^1 = 180°$, $\chi^2 = +90°$ state. The $\chi^1$ values are dictated by intraresidue $H_\alpha$–$H_\beta$ NOEs and coupling constants (Fig. 1). $\chi^2$ values are directly influenced only by NOE constraints. The normal to the indole plane of $Trp^{15}$ is within 20° of being perpendicular to the helical axis, while the $Trp^{11}$ normal is within 20° of being parallel. $Trp^9$ and $Trp^{13}$ are intermediate in this respect, with angles of 40–50° from the axis. The planes of $Trp^9$ and $Trp^{11}$ from different monomers overlap slightly. No other tryptophan intermolecular contacts are suggested by the structures. Even here, NOEs are not

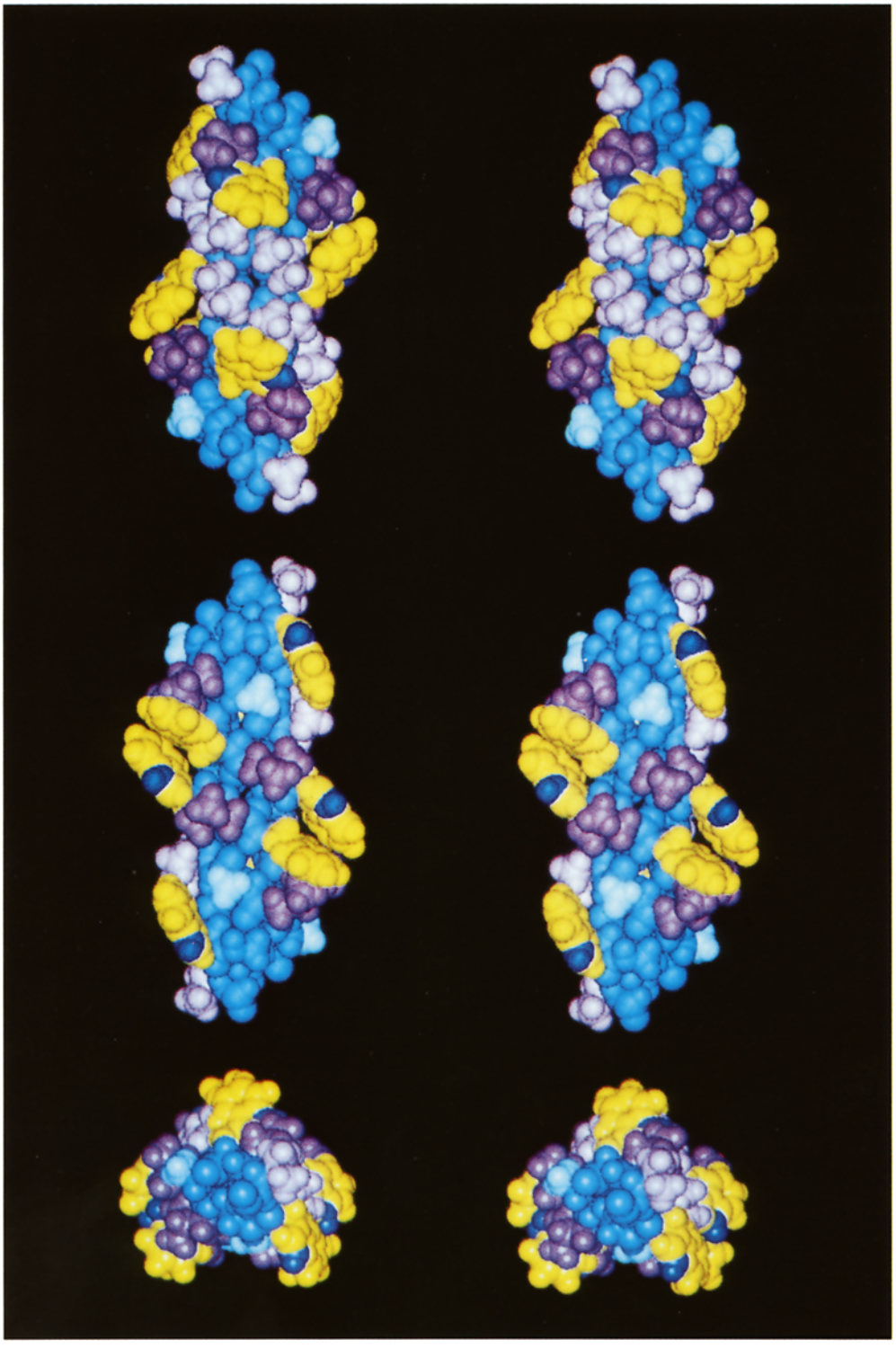

TABLE 2
TORSION ANGLES FOR SPECIES 3 IN BENZENE/ETHANOL

| Residue | $\phi$ | $\psi$ | $\chi^1$ or $\Theta_{N\text{-}H_\beta}$ [a] | $\chi^2$ or $\Theta_{C_\alpha\text{-}H_\gamma}$ [b] |
|---|---|---|---|---|
| $Val^1$ | −99 ± 1 | 112 ± 9 | −179 ± 7 | |
| $Ala^3$ | −152 ± 8 | 105 ± 9 | | |
| $Ala^5$ | −154 ± 10 | 113 ± 10 | | |
| $Val^7$ | −153 ± 11 | 117 ± 6 | 38 ± 7 | |
| $Trp^9$ | −152 ± 6 | 107 ± 13 | −136 ± 1 | −65 ± 4 (2) |
| $Trp^{11}$ | −149 ± 12 | 115 ± 7 | 142 ± 4 | 38 ± 2 |
| $Trp^{13}$ | −160 ± 6 | 117 ± 14 | −156 ± 4 | −45 ± 3 |
| $Trp^{15}$ | −165 ± 6 | 82 ± 14 | −170 + 6 | −77 ± 6 |
| $Gly^2$ | 106 ± 12 | −147 ± 8 | | |
| $Leu^4$ | 110 ± 5 | −144 ± 10 | 90 ± 6 | −93 ± 9 (2) |
| $Val^6$ | 104 ± 6 | −144 ± 10 | 57 ± 3 | |
| $Val^8$ | 104 ± 3 | −144 ± 5 | 169 ± 8 | |
| $Leu^{10}$ | 109 ± 7 | −149 ± 11 | 68 ± 15 | −45 ± 15 (6) |
| $Leu^{12}$ | 102 ± 5 | −135 ± 6 | 133 ± 2 (2) | 41 ± 9 (1) |
| $Leu^{14}$ | 111 ± 12 | −137 ± 4 | 74 ± 4 | 124 ± 2 |

[a] Entries in this column for valine represent $\Theta_{N\text{-}H_\beta}$ in order to avoid any possible ambiguities in the definition of $\chi^1$. All other entries represent $\chi^1$.

[b] Entries in this column for leucine represent $\Theta_{C_\alpha\text{-}H_\gamma}$ in order to avoid any possible ambiguities in the definition of $\chi^2$. All other entries represent $\chi^2$.

'±' indicates root-mean-square deviation (rmsd).

'( )' indicates the number of structures (out of 15) which do not fall near this rotamer, and thus are not included in the calculation for this angle.

assigned between these two rings, because of the lack of chemical-shift dispersion among the indole ring protons of the four tryptophans per gramicidin monomer. The small degree of ring stacking is a surprising result for a peptide with effectively 30 amino acids and eight tryptophans. The antiparallel helix serves to segregate tryptophan residues (nos. 9, 11, 13 and 15) from different monomers to opposite ends of the helix. Tryptophans from the same monomer are effectively spaced by intervening leucines, and for $Trp^9$ and $Trp^{15}$ by an intervening molecule. Only toward the center of the helix can two pairs ($Trp^9$ and $Trp^{11}$) interact.

Most of the tryptophan side chains are thus closely associated with one or more D-leucine side chains. $Leu^4$, $Leu^{10}$ and $Leu^{14}$ values have converged to near the $\chi^1 = +60°$ rotamer (Table 2), as dictated by intraresidue $H_\alpha$–$H_\beta$ NOEs and coupling constants (Table 1). This corresponds to the most common L-leucine $\chi^1$ value of −60° found in X-ray crystallography studies of proteins (Bhat et al., 1979), which is usually accompanied by $\Theta_{C\alpha H\gamma} = +60°$ for L-leucine, corresponding to

←

Fig. 5. CPK views of one of the 15 structures from Fig. 4: (a, top) hydrophobic face. Note the tight packing of valine and tryptophan side chains in the center. (b, middle) hydrophilic face. Only $Ala^5$ and $Leu^{10}$ side chains block solvent access to the backbone. (c, bottom) axial view, with hydrophilic face at the bottom of the figure. Four Trp indole-HN groups also project toward this face. Color key: medium blue, backbone; yellow, tryptophan; purple, valine; pink, leucine; aqua, alanine; dark blue, indole-HN (stereoview).

$\Theta_{C\alpha H\gamma} = -60°$ for D-leucine. (In the present study, $\Theta_{C\alpha H\gamma}$ is used in place of $\chi^2$ for D-leucine to avoid possible ambiguities in the definition of $\chi^2$ arising from stereodefinition of the methyl groups in D-amino acids. Similarly, $\Theta_{N\text{-}H\beta}$ is used in place of $\chi^1$ for all valines.) Leu[4] and Leu[10] $\Theta_{C\alpha H\gamma}$ values fall close to the $-60°$ rotameric state. Leu[12] $\chi^1$ is not as well constrained due to the chemical-shift degeneracy of its β-protons. The ends of the Trp[9] rings come into close contact with the Leu[12] methyl groups from the opposite strand. Both methyl groups from Leu[4] pack into the face of the Trp[11] ring. Trp[11] also closely contacts one methyl from Leu[12] in the plane of the ring. Trp[13] and Leu[14] are packed closely in a similar arrangement. These planar contacts can be used to interpret the downfield shift of one methyl group in both Leu[12] and Leu[14] (Table 1). Trp[15] avoids this type of intimate contact by virtue of its position at the end of the helix.

Each of the valines has also converged to a single rotamer (Table 2, Fig. 4), although only one of these rotamers (Val[7], $\Theta_{N\text{-}H\beta} \approx 60°$) corresponds to the one most commonly found in crystallographic studies (Bhat et al., 1979). Toward the center of one face of the dimer, four valines (both Val[7] and Val[8], Fig. 5a) are surrounded by four tryptophans (Trp[13] above and below, and Trp[9] left and right). A combination of these interactions, together with interactions between the valines,

TABLE 3
VIOLATIONS OF NOE CONSTRAINTS

| | Number of NOE violations[a] | | | Rms NOE violations (Å) | | |
|---|---|---|---|---|---|---|
| bb number | bb–bb | bb–sc | sc–sc | bb–bb | bb–sc | sc–sc |
| 1 | 0 | 14 | 26 | 0.01 | 0.41 | 0.73 |
| | | 14 | 28 | | 0.42 | 0.71 |
| | | 12 | 25 | | 0.42 | 0.72 |
| 2 | 0 | 10 | 23 | 0.01 | 0.40 | 0.75 |
| | | 10 | 23 | | 0.40 | 0.75 |
| 3 | 3 | 10 | 20 | 0.02 | 0.42 | 0.70 |
| 4 | 3 | 12 | 24 | 0.02 | 0.43 | 0.71 |
| | | 14 | 24 | | 0.43 | 0.70 |
| | | 14 | 24 | | 0.43 | 0.70 |
| | | 12 | 24 | | 0.43 | 0.71 |
| | | 12 | 24 | | 0.43 | 0.71 |
| 5 | 2 | 12 | 25 | 0.02 | 0.43 | 0.68 |
| | | 12 | 22 | | 0.41 | 0.68 |
| | | 10 | 24 | | 0.41 | 0.69 |
| 6 | 1 | 10 | 22 | 0.02 | 0.42 | 0.72 |
| Averages | | | | | | |
| | 1.5 | 11.9 | 23.7 | 0.01 | 0.42 | 0.71 |

The first column indicates which of the six backbone structures was used as a scaffold for side-chain conformational analysis.

Other columns list data for violations of three types of NOEs:

- (bb–bb) between two backbone protons (212 NOEs)
- (bb–sc) between backbone and side chain (264 NOEs)
- (sc–sc) between two side-chain protons (184 NOEs)

[a] (bb–bb) NOE violations are counted if > 0.1 Å. (bb–sc) and (sc–sc) NOE violations are counted if > 1.0 Å.

could provide a barrier to free rotation about the $C_\alpha$–$C_\beta$ bond. Val[6] is just outside this region, with its β-proton oriented towards this valine cluster. Val[1] is at the end of the helix. Its β-proton is oriented inwards to the helix, with the methyl groups oriented toward the helical ends.

On the opposite side of the helix (Fig. 5b), a large relatively side-chain-free groove exists, where only four side chains, from both Leu[10] and Ala[5] residues, are situated. This open space may allow Leu[10] to reorient. This would help to explain the relatively high rmsd of the Leu[10] $\chi^1$ and $\Theta_{C_\alpha H_\gamma}$ values in Table 2. Note that six of the structures have $\Theta_{C_\alpha H_\gamma}$ values well outside the quoted range near 45°. The full dispersion of the Leu[10] residues can be seen in Fig. 4, in profile between the Trp[11] indoles. Another consequence of the Leu[10] isolation is the presence of only a few NOEs between Leu[10] and other side chains, which adds to the uncertainty in its position. Lack of close contacts with tryptophan leaves the methyl chemical shifts upfield in a crowded region, and not well dispersed. Only four NOEs were positively identified between Leu[10] side chains and other side-chain atoms. All of these factors contribute to preventing a stereospecific assignment of the Leu[10] methyl groups.

The groove creates a relatively hydrophilic face, due to exposure of the backbone hydrogen bonds. The Trp[9] and Trp[15] residues are positioned with their indole-HN groups toward this face, increasing the hydrophilicity. It is likely that solvent ethanol interacts predominantly with this face, and benzene is attracted more strongly to the other three (hydrophobic) cylindrical quadrants.

*Dynamics*

The presence of significant backbone dynamics is not required to explain the backbone NOEs and coupling constants. The average rms violation of NOEs between backbone atoms is 0.01 Å for the six structures in Fig. 3 (Table 3). There are no dihedral violations (ϕ constraints) of more than 1°. In short, the backbone is very well determined and relatively static, even at the ends of the structure.

The side chains are considerably less static. Although the rmsd of $\chi^1$ and $\chi^2$ values is small (Table 2), NOE rms violations are almost two orders of magnitude higher for NOEs involving side chains than for those within the backbone (Table 3). A single conformation cannot satisfy all of the side-chain NOEs, thus multiple conformations must be present. These conformations must be sampled quickly on the NMR time scale (much greater than 100 Hz), or they would give rise to multiple chemical shifts for individual atoms. Therefore, the side-chain structures depicted in Fig. 4 represent crude time-averaged conformations resulting from time-averaged coupling constants and NOEs. This also applies to the backbone, but the amplitude of motion is much smaller, or a single conformation is much more heavily weighted, as dictated by the lack of significant NOE violations.

Initial structure calculations introduced the backbone and side-chain constraints simultaneously according to standard practice, but this only resulted in an unwarranted disruption of the backbone structure without noticeable improvement to the side-chain conformations. Large violations of backbone constraints were observed, as well as destruction of the symmetry required by the uniformity of the backbone coupling constants and NOEs (Table 1; see also Zhang et al., 1992, Table 2). For instance, a proton from a Trp[13] exhibits NOEs to two parts of the backbone which cannot simultaneously be satisfied, causing these points to be drawn closer during the annealing (Fig. 6). A simple torsional change in $\chi^2$ was used to generate a second hypothetical

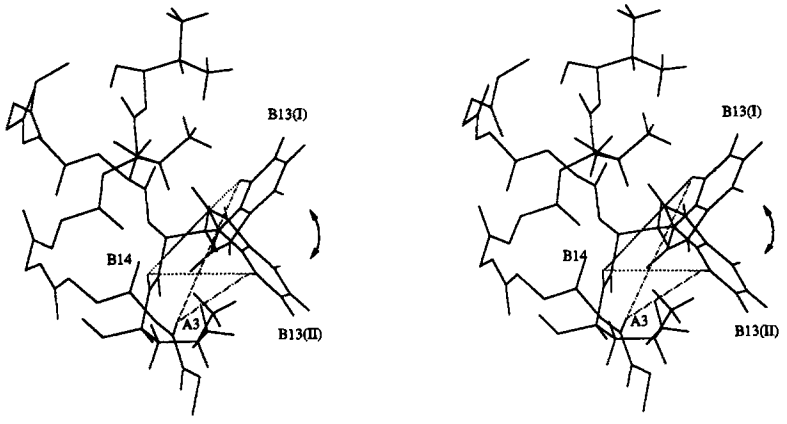


Fig. 6. Example of a possible dynamic motion of a tryptophan ring. B13(I) is the conformation calculated for monomer A $Trp^{13}$ by distance geometry/simulated annealing. B13(II) is a second conformation, generated by a simple $\chi^2$ rotation of 103°, in order to satisfy two large NOE violations between B13(I) and two amide protons. This torsion changes the distance between $H_\varepsilon$(A13) and HN(A14) from 5.5 to 4.5 Å, and the distance between $H_\varepsilon$(13) and HN(B3) from 6.3 to 4.0 Å (dotted lines). A dynamic equilibrium between these two structures represents one possible interpretation of the data.

position for $Trp^{13}$ which satisfies the two largest NOE violations. It seems unreasonable to allow the NOEs from the dynamic side chains to influence the structure of the backbone, and therefore in this study the backbone was fixed during side-chain calculations. This type of problem may be common to many structure calculations when regions of dissimilar dynamic properties exist. Consequently, the protocol developed here may have general applicability to surface-exposed side chains that are well recognized as being flexible. Furthermore, this approach may be appropriate for handling loop structures where backbone and side-chain sites are flexible while the rest of the protein is relatively well defined.

Figure 7 charts the total number of NOEs involving side-chain protons (top) and the rms violation of these NOEs (bottom) for each residue. Violation of an NOE between two side-chain protons (sc–sc, light gray bars) could result from dynamics of either or both side chains. Violation of NOEs between side-chain protons and the relatively static backbone can be used to assign dynamic behavior to individual side chains. Furthermore, large violation of NOEs between β-protons and the backbone (β–bb, black bars) can be used to analyze $\chi^1$ torsional motion. In the absence of $\chi^1$ dynamics, violation of NOEs between other side-chain atoms and the backbone (γ+–bb, dark gray bars) would indicate $\chi^2$ torsional motion.

Of 110 β–bb NOEs (220 for the dimer) only three large violations cannot be satisfied by rotation of some torsion about $\chi^1$: $H_\beta(6)$–HN(7), $H_\beta(6)$–$H_\alpha(10)$ and $H_\beta(3)$–$H_\alpha(13)$. These violations give rise to the black bars for $Val^6$ and $Ala^3$ in the bottom half of Fig. 7. Interestingly, the largest $^3J_{N\alpha}$ measured is for $Val^6$ and the smallest is for $Trp^{13}$. These discrepancies could indicate backbone distortions which were not detected in the backbone refinement. These specific NOE violations then do not necessarily represent $\chi^1$ dynamics. Possibly a distortion or kink in the backbone is present that was not adequately determined by the backbone constraints used for backbone refinement.

The β–bb NOE violations for the remainder of the residues indicate considerable tryptophan $\chi^1$ dynamics, particularly in the cases of $Trp^{11}$ and $Trp^{15}$. These NOEs can be satisfied, though not

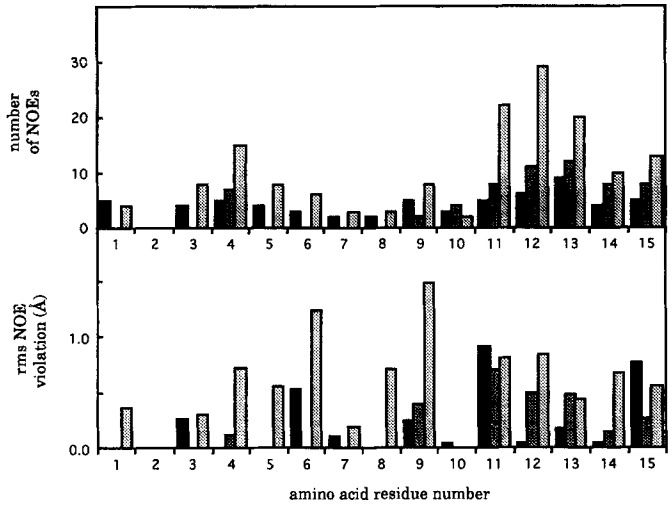


Fig. 7. Number of side-chain NOEs assigned per residue (top), and average side-chain NOE rms violation per residue (bottom). Black bars represent NOEs between β-protons of the specified residue and the backbone (β–bb). Dark gray bars represent NOEs between other protons of the specified side chain and the backbone (γ+–bb). Light gray bars represent side-chain–side-chain (sc–sc) NOEs. These violations can be used to qualitatively interpret localized dynamic motion.

simultaneously, by a rotamer distribution about $\chi^1$. In order to investigate $\chi^1$ dynamics, it is useful to assume populations of only the three $\chi^1$ staggered rotameric states ($\chi^1 = 180°$, $+60°$, $-60°$). By means of a calculation of partial populations of each of these rotamers, an attempt to match the β–bb NOEs and the $^3J_{\alpha\beta}$ values can be made. For instance, the theoretical value of $^3J_{\alpha\beta 3}$ for tryptophan is $13 \times P(180°) + 3.5 \times P(+60°) + 3.5 \times P(-60°)$ where $P(\chi^1)$ represents the occupational probability of that rotamer. An NOE is taken as evidence of population for a specific rotamer if only that rotamer can satisfy the distance constraint. Reduction of this NOE by, for instance, a factor of 10 due to partial occupation increases the calculated distance by a factor of only 1.46 due to the $r^{-6}$ dependence of NOEs. This small factor of 1.46 could permit population of rotameric states in the simulation which are not actually populated in the molecule. However, if only a single rotamer can satisfy the NOE, then population of that rotamer is confirmed.

The results of this analysis are shown in Table 4. $Trp^9$, $Trp^{13}$ and $Trp^{15}$ predominantly occupy the $\chi^1 = 180°$ rotamer, with minor occupation of $\chi^1 = +60°$. $Trp^{11}$ is also predominantly in the $\chi^1 = 180°$ rotamer, but with minor occupation of $\chi^1 = -60°$ required. Slight occupation of the third rotamer is also possible, especially for $Trp^9$ and $Trp^{11}$. A similar analysis of D-leucine sites predicts dominant occupation of $\chi^1 = +60°$ for $Leu^4$, $Leu^{10}$ and $Leu^{14}$. $Leu^{10}$ data suggest additional occupation of $\chi^1 = -60°$, while minor occupations of $Leu^4$ and $Leu^{14}$ are not as clear. No large $H_\beta$–backbone NOE violations were detected for any D-amino acid (even numbers) other than $Val^6$, for which the backbone may be imperfect as described above. This does not necessarily imply that no $\chi^1$ dynamics are present. Rather, it results from a difference in the geometry of L- vs. D-sites, which affects the NOE information available. Of course, librations within a rotameric state or quasistatic displacements from the equilibrium values of $\chi^1$ cannot be measured or precluded by this qualitative analysis, and could be responsible for changes in coupling-constant values, particularly when no NOE evidence exists for additional rotamers.

The existence of one large and one small $^3J_{\alpha\beta}$ value was recorded for each tryptophan and leucine residue. Free rotation or three-site jumps of equal occupation would be expected to produce two nearly equal intermediate coupling values, due to time-averaging of large and small couplings. The values of tryptophan and leucine $^3J_{\alpha\beta}$ in Table 1 thus preclude the possibility of freely rotating side chains or equal occupation of three-site $\chi^1$ jumps. $\chi^1$ dynamics of the remaining side chains are not as well defined. Ala[3] and Ala[5] are assumed to rotate freely (or by rapid three-site jumps of equal average occupation). The chemical shifts of Leu[12] β-protons are degenerate, which prevents stereospecific measurement of coupling constants or NOEs. Valines have only one β-proton and hence one $^3J_{\alpha\beta}$ coupling constant. The value of this constant is intermediate for all four valines, which reduces the usefulness of the data. This could indicate free rotation, two- or three-site jumps or static off-rotamer occupation. In addition, Val[7] and Val[8] are positioned in the center of the helix, where they are in contact with each other and with Val[7] and Val[8] from the second chain. Intramolecular and intermolecular NOEs cannot be distinguished in these cases. Chemical shifts of the methyl groups of Val[6], Val[7] and Val[8] are tightly grouped in a crowded region of the spectrum, further complicating NOE detection. Thus, these methyl groups were not stereospecifically assigned, and resolved constraints are few (Fig. 7). Val[1] is the terminal residue at the 'sticky end' of the helix. As seen in Figs. 3 and 4 the N-terminus is highly exposed relative to the C-terminus and consequently it has solvent-exposed hydrogen-bonding potential (hence the term 'sticky end'). A distribution about $\chi^1$ which includes rotation of $H_\beta$ past the end of the helix would not necessarily create additional NOEs to $H_\beta$, since no additional protons are present. Constraints to the methyl protons are weakened by 2.3 Å due to chemical-shift degeneracy which requires use of a pseudoatom in addition to multiplicity considerations, hence their orientation is less certain. The degeneracy of the methyl groups together with an intermediate $^3J_{\alpha\beta}$ value helps to support the notion of free rotation or equal occupational three-site jumps of Val[1] $\chi^1$.

TABLE 4
$\chi^1$ ROTAMER POPULATIONS

| Residue | Number | Data type | $\chi^1$ rotamer (°) | | | Residue | Number | Data type | $\chi^1$ rotamer (°) | | |
|---|---|---|---|---|---|---|---|---|---|---|---|
| | | | 180 | +60 | −60 | | | | 180 | +60 | −60 |
| D-Leu | 4 | $^3J_{\alpha\beta}$ | m− | D | m− | L-Trp | 9 | $^3J_{\alpha\beta}$ | D | m | m− |
| | | β–bb NOE | | * | | | | β–bb NOE | * | * | |
| | | Result | | D | | | | Result | D | m | |
| | 10 | $^3J_{\alpha\beta}$ | | D | m | | 11 | $^3J_{\alpha\beta}$ | D | m− | m |
| | | β–bb NOE | | * | | | | β–bb NOE | * | | * |
| | | Result | | D | m | | | Result | D | | m |
| | 14 | $^3J_{\alpha\beta}$ | m− | D | m− | | 13 | $^3J_{\alpha\beta}$ | D | m | |
| | | β–bb NOE | | * | | | | β–bb NOE | * | * | |
| | | Result | | D | | | | Result | D | m | |
| | | | | | | | 15 | $^3J_{\alpha\beta}$ | D | m | |
| | | | | | | | | β–bb NOE | * | * | |
| | | | | | | | | Result | D | m | |

D represents the dominant rotamer (> 60%); m indicates minor occupation (20–40%); m− indicates very minor occupation (< 20%). The three rows for each residue indicate rotamer populations derived by analysis of 1. $^3J_{\alpha\beta}$ values; 2. βH–backbone NOEs; 3. result of a conservative analysis of a combination of $^3J_{\alpha\beta}$ and βH–backbone NOEs.

## CONCLUSIONS

Separating the backbone and side-chain NOEs has proven to be very useful. The closest interface between these NOE types, β–bb NOEs, becomes an effective tool for assessing local dynamics, ultimately helping to refine the structure. The backbone may contain a few slight imperfections due to omission of NOEs involving side chains, but these are significantly less detrimental than the large distortions which result from including side-chain NOEs. These imperfections could be reduced somewhat by including β–bb NOEs in the backbone calculation, in the form of pseudoatom constraints. The pseudoatoms should be designed in such a way that each β–bb NOE-derived constraint is unaffected by $\chi^1$ torsions, so that $\chi^1$ dynamics do not result in a falsely altered backbone structure. Other structure determinations which also involve separate regions of minimal and appreciable dynamics may benefit from a similar approach.

The combination of NOE and J-coupling data for three leucines and four tryptophans clearly identifies a dominant rotamer for each residue. Furthermore, the distance geometry/simulated annealing structures have $\chi^1$ angles within 45° of this dominant rotamer (and usually much closer). Consequently, the side-chain conformations determined are indeed useful despite the fact that they represent time-averaged structures. What is somewhat misleading about these structures is the remarkable rmsd of the $\chi^1$ torsion angles which is as small as 1° for $Trp^9$. This merely documents that structures with minimal violation of the time-averaged constraints have been reproducibly achieved. Furthermore, $\chi^2$ jumps would be expected to accompany the $\chi^1$ jumps (Mack et al., 1988; Karpen et al., 1993). Therefore, these side-chain structures represent excellent qualitative (i.e. dominant rotameric state) information, at least for $\chi^1$, but a highly refined structure must include a detailed dynamics analysis. Relaxation studies could provide complementary information.

The species 3 structure in benzene/ethanol is known to convert readily to the channel state in a lipid environment (Moll and Cross, 1990). It is clear from the structure determined here that, in the absence of a structural conversion, the distribution of tryptophans along the helical axis would result in the burial of several hydrophilic indole NH groups deep within the lipid bilayer. It has been suggested that removal of these NH groups from the bilayer center is a significant component of the driving force for the conversion to the channel state (Zhang et al., 1992). The preferential orientation of the indole NH groups toward the hydrophilic cleft indicates that the tendency of the indole group to seek a more polar environment can influence the structure. This solvent-exposed cleft may also directly participate in the conformational conversion. Breaking of hydrogen bonds to achieve the conversion requires exposure of the backbone to a catalytic solvent. Clearly the pore in this structure is not large enough to permit solvent access to the backbone, but the cleft appears to be adequate. The amphipathic nature of the structure could be due in part to the amphipathic nature of the solvent. Different regions of the molecular surface appear tailored to interact with apolar benzene molecules, or with the more polar ethanol molecules. The species 3 backbone motif creates a scaffold which allows a parting of the side chains to expose the backbone and create the cleft. The amphipathic nature of this helix may be a factor leading to species 3 domination of the conformational equilibrium between double helices in benzene/ethanol.

## ACKNOWLEDGEMENTS

The staff of the FSU NMR Facility, Joseph Vaughn, Richard Rosanske and Thomas Gedris, are gratefully acknowledged for their skillful maintenance of the VXR500 NMR spectrometer. The staff of the FSU Bioanalytical Services and Synthesis Facility, Hank Henricks and Umesh Goli, are also gratefully acknowledged. S.M.P. acknowledges the support of a University Fellowship. T.A.C. extends his appreciation for partial financial support of this work to NIH grant AI-23007.

## REFERENCES

Anderson, O. (1984) *Annu. Rev. Physiol.*, **46**, 531–548.
Arseniev, A.S., Bystrov, V.F., Ivanov, V.T. and Ovchinnikov, Y.A. (1984) *FEBS Lett.*, **165**, 51–56.
Baker, E.N. and Hubbard, R.E. (1984) *Prog. Biophys. Mol. Biol.*, **44**, 97–179.
Bano, M. de C., Braco, L. and Abad, C. (1989) *FEBS Lett.*, **250**, 67–71.
Bax, A. and Davis, D.G. (1985) *J. Magn. Reson.*, **65**, 355–360.
Bhat, T.N., Sasisekharan, V. and Vijayan, M. (1979) *Int. J. Pept. Protein Res.*, **13**, 170–184.
Bodenhausen, G. and Ernst, R.R. (1982) *Mol. Phys.*, **47**, 319–328.
Braco, L., Abad, C., Campos, A. and Figueruelo, J.E. (1986) *J. Chromatogr.*, **353**, 181–182.
Braunschweiler, L. and Ernst, R.R. (1983) *J. Magn. Reson.*, **53**, 521–528.
Breeze, A.L., Harvey, T.S., Bazzo, R. and Campbell, I.D. (1991) *Biochemistry*, **30**, 575–582.
Brown, J.E. and Klee, W.A. (1971) *Biochemistry*, **10**, 470–476.
Brüschweiler, R., Blackledge, M. and Ernst, R.R. (1991) *J. Biomol NMR*, **1**, 3–11.
Bystrov, V.F. and Arseniev, A.S. (1988) *Tetrahedron*, **44**, 925–940.
Demarco, A., Clinas, M. and Wüthrich, K. (1978) *Biopolymers*, **17**, 617–636.
Dyson, H.J., Cross, K.J., Ostresh, J., Houghten, R.A., Wilson, I.A., Wright, P.E. and Lerner, R.A. (1985) *Nature*, **318**, 480–483.
Dyson, H.J., Rance, M., Houghten, R.A., Lerner, R.A. and Wright, P.E. (1988) *J. Mol. Biol.*, **201**, 161–200.
Eberle, W., Pastore, A., Sander, C. and Rosch, P. (1991) *J. Biomol. NMR*, **1**, 71–82.
Fields, C.G., Fields, G.B., Noble, R.L. and Cross, T.A. (1989) *Int. J. Pept. Protein Res.*, **33**, 298–303.
Fisher, R. and Blumenthal, T. (1982) *Proc. Natl. Acad. Sci. USA*, **79**, 1045–1048.
Jeener, J., Meier, B.H., Bachmann, P. and Ernst, R.R. (1979) *J. Chem. Phys.*, **71**, 4546–4553.
Karpen, M.E., Tobias, D.J. and Brooks III, C.L. (1993) *Biochemistry*, **32**, 412–420.
Katsaras, J., Prosser, R.S., Stinson, R.H. and Davis, J.H. (1992) *Biophys. J.*, **61**, 827–830.
Katz, E. and Demain, A.L. (1977) *Bacteriol. Rev.*, **41**, 449–474.
Killian, J.A. (1992) *Biochim. Biophys. Acta*, **1113**, 391–425.
Killian, J.A., Nicholson, L.K. and Cross, T.A. (1988a) *Biochim. Biophys. Acta*, **943**, 535–540.
Killian, J.A., Prasad, K.U., Hains, D. and Urry, D.W. (1988b) *Biochemistry*, **27**, 4848–4855.
Kim, Y. and Prestegard, J.H. (1989) *J. Magn. Reson.*, **84**, 9–13.
Kumar, A., Ernst, R.R. and Wüthrich, K. (1980) *Biochem. Biophys. Res. Commun.*, **95**, 1–6.
Langs, D.A. (1988) *Science*, **241**, 188–191.
Langs, D.A., Smith, G.D., Courseille, C., Precigoux, G. and Hospital, M. (1991) *Proc. Natl. Acad. Sci. USA*, **88**, 5345–5349.
LoGrasso, P.V., Moll III, F. and Cross, T.A. (1988) *Biophys. J.*, **54**, 259–267.
Lynch, B. and Kaiser, E.T. (1988) *Biochemistry*, **27**, 7600–7607.
Mack, J.W., Torschi, D.A. and Steinert, P.M. (1988) *Biochemistry*, **27**, 5418–5426.
Mitchell, J.B.O. and Price, S.L. (1990) *J. Comput. Chem.*, **11**, 1217–1233.
Moll III, F. and Cross, T.A. (1990) *Biophys. J.*, **57**, 351–362.
Mueller, L. (1987) *J. Magn. Reson.*, **72**, 191–196.
Nicholson, L.K. and Cross, T.A. (1989) *Biochemistry*, **28**, 9379–9385.

Nilges, M., Clore, G.M. and Gronenborn, A.M. (1988) *FEBS Lett.*, **229**, 317–324.
Nilges, M., Kuszewski, J. and Brunger, A.T. (1992) *X-PLOR Manual*, version 3.0.
Pascal, S.M. and Cross, T.A. (1992) *J. Mol. Biol.*, **226**, 1101–1109.
Pascal, S.M. and Cross, T.A. (1993) *Life Sci. Adv. Biophys.*, in press.
Piantini, O.W., Sørensen, O.W. and Ernst, R.R. (1982) *J. Am. Chem. Soc.*, **104**, 6800–6801.
Ramachandran, G.N. and Chandrasekaran, R. (1972) *Indian J. Biochem. Biophys.*, **9**, 1–11.
Rance, M., Bodenhausen, G., Wagner, G., Wüthrich, K. and Ernst, R.R. (1985) *J. Magn. Reson.*, **62**, 497–510.
Roux, B., Bruschweiler, R. and Ernst, R.R. (1990) *Eur. J. Biochem.*, **194**, 57–60.
Sarkar, N., Langley, D. and Paulus, H. (1977) *Proc. Natl. Acad. Sci. USA*, **74**, 1478–1482.
Shaka, A.J. and Freeman, R. (1983) *J. Magn. Reson.*, **51**, 169–173.
States, D.J., Haberkorn, R.A. and Ruben, D.J. (1982) *J. Magn. Reson.*, **48**, 286–292.
Summers, M.F., South, T.L., Kim, B. and Hare, D. (1990) *Biochemistry*, **29**, 329–340.
Torda, A.E., Scheek, R.M. and Van Gunsteren, W.F. (1990) *J. Mol. Biol.*, **214**, 223–235.
Veatch, W.R., Fossel, E.T. and Blout, E.R. (1974) *Biochemistry*, **13**, 5249–5256.
Williamson, M.P., Hall, M.J. and Handa, B.K. (1986) *Eur. J. Biochem.*, **158**, 527–536.
Wüthrich, K., Billeter, M. and Braun, W. (1983) *J. Mol. Biol.*, **169**, 949–961.
Zhang, Z., Pascal, S.M. and Cross, T.A. (1992) *Biochemistry*, **31**, 8822–8828.